Journal of Power Sources 247 (2014) 481–488

Contents lists available at ScienceDirect

Journal of Power Sources

journal homepage: www.elsevier.com/locate/jpowsour

Computationally-efficient hybrid strategy for mechanistic modeling of fuel cell stacks

A.K. Sharma [a], E. Birgersson [a, *], S.H. Khor [b]

[a] Department of Chemical and Biomolecular Engineering, National University of Singapore, Singapore 117576, Singapore
[b] Department of Mechanical Engineering, National University of Singapore, Singapore 117575, Singapore

HIGHLIGHTS

- A hybrid strategy is proposed for mechanistic modeling of fuel cell stacks.
- The strategy is verified with the full set of equations for a 10-cell stack.
- The strategy preserves geometrical resolution and captures essential physics.
- In particular, captures redistribution of current and heat flux across the cells.
- 80% reductions in computational cost; allows for simulation of large stacks.

ARTICLE INFO

Article history:
Received 9 June 2013
Received in revised form
19 August 2013
Accepted 23 August 2013
Available online 6 September 2013

Keywords:
Fuel cell stacks
Mechanistic modeling
Model reduction
Space marching
Hybrid strategy

ABSTRACT

In general, detailed mechanistic models for fuel cell stacks that seek to capture the local transport phenomena are computationally expensive. In this context, we propose a hybrid modeling strategy, in which the steady-state conservation equations are solved iteratively in two separate groups: The first comprises asymptotically-reduced governing equations for momentum, mass, and species, which are solved as a transient-like propagation problem; the second comprises the full set of equations for energy and charge, which are solved as an elliptic stationary problem. Physically, the segregation is justified by the nature of the dependent variables; in essence, the first group covers local variables on the cell level and the second involves global variables on the stack level. We demonstrate the methodology for a steady-state detailed mechanistic model of a proton exchange membrane fuel cell stack comprising 2 to 350 cells subjected to non-uniform operating conditions across the cells; e.g., a stack comprising 350 cells takes less than an hour to solve. The proposed methodology is generic and can also be employed for other systems where transport phenomena occur on different length scales and involve some form of slenderness.

1. Introduction

Mathematical modeling and simulation have found widespread use in the research and development of fuel cells; however, the majority of detailed mechanistic models that provide geometrical resolution and resolve the essential physics have focused on the cell level so far [1–8]. At the stack level, only a few detailed mechanistic models can be found [9–18], which are limited to small stacks of up to around 5 to 10 cells. Modeling of larger stacks generally involves simplifications [19–37] with a loss in the level of detail and resolution of the salient features of the electrochemical and transport phenomena.

In essence, detailed mechanistic models typically consider conservation of mass, momentum, species, energy and charge in the form of a system of coupled nonlinear elliptic partial differential equations (PDEs) with the relevant boundary conditions and constitutive relations to ensure a well-posed problem. While these models can be solved reasonably fast and efficiently for a single cell, the associated computational cost for stacks quickly becomes prohibitive because of the large number of functional domains-separator plates (sp), gas flow fields (ff), coolant flow fields (cff), porous backings (pb), catalyst layer (cl), electrolyte (el) – in each and every cell in a stack (see Fig. 1). One strategy to deal with such large simulations is to deploy clusters of computers or other types of parallel computing environments to speed up calculations, yet these simulations still take on the order of hours or days for fuel cell stacks [1,7,12,25,28,38–40]. Another possible strategy to reduce the overall complexity and associated computational cost of a stack

* Corresponding author. Tel.: +65 6516 7132; fax: +65 6775 4710.
E-mail address: chebke@nus.edu.sg (E. Birgersson).

0378-7753/$ – see front matter © 2013 Elsevier B.V. All rights reserved.
http://dx.doi.org/10.1016/j.jpowsour.2013.08.094

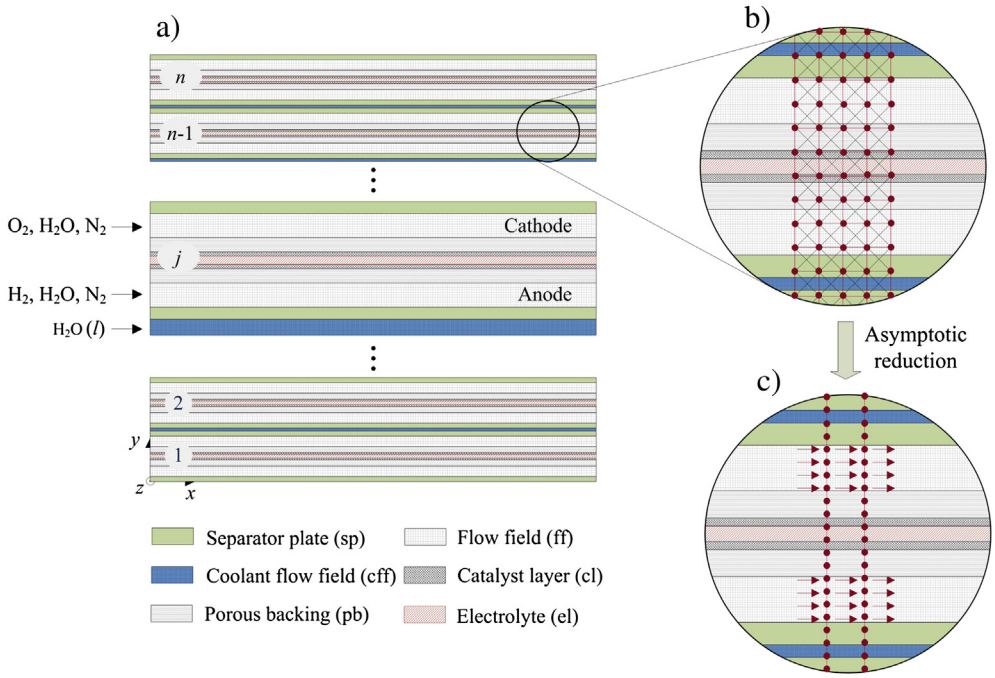

Fig. 1. Schematic for a PEMFC stack comprising n cells, denoted by j (a); mathematical nature of the governing equations for the full stack model (b) and reduced stack model (c): elliptic PDEs (⊠), parabolic PDEs (→) and ODEs (|).

model is to address the underlying mathematical nature of the system of equations. Care has to be taken though so as not to reduce the fidelity of model predictions especially when reductions sacrifice leading-order phenomena or dimensionality. This strategy was demonstrated in Refs. [41], where a leading-order reduced mathematical model for a proton exchange membrane fuel cell (PEMFC) stack was derived and shown to cut down the computational cost by 2–3 orders of magnitude (depending on stack size). The leading-order solution was, however, found to be unable to capture the redistribution of physical quantities for stacks subjected to significant perturbations between cells—a key phenomenon in fuel cell stacks [42–44].

In light of the promise the reduced model [41] holds in terms of computational efficiency even for large stacks of hundreds of cells or more, we shall here seek to overcome its main limitation by exploring a hybrid strategy that exploits the inherent nature of the dependent variables. In short, we shall argue that the dependent variables exist either locally in each cell or globally throughout the stack whence their PDEs can be split up into two separate groups. The local variables can now be solved at leading order with a space-marching algorithm whilst the global are allowed to retain their elliptic nature; iteration between the two groups then links them together into a complete stack model. We demonstrate the proposed strategy for the steady-state operation of a 10-cell PEMFC stack subject to non-uniform operating conditions for the individual cells.

The layout of the paper is as follows. First, we introduce the mathematical formulation for the full and proposed hybrid model for a PEMFC stack, which is then followed by a summary of the hybrid coupling methodology. After a description of numerics necessary to solve the models, the results of the hybrid model for both the global and local behavior are verified against those of the full model. The savings in computational cost in terms of memory usage and computing time are then discussed. Finally, we draw conclusions and highlight how the present approach can be adapted to other systems.

2. Mathematical formulation

Let us start by turning our attention towards a typical fuel cell stack as illustrated schematically in Fig. 1, which comprises several single cells connected in series; each cell further contains several functional layers. A detailed mechanistic model needs to consider coupled transport phenomena – mass, momentum, species, energy, and charge – in all of the relevant length scales that can be found in the stack. Since the cells in a stack are connected via impermeable graphite or metallic plates, transport of mass, momentum, and species is confined to individual cells; in contrast, the transport of energy and charge occurs across the cells and throughout the entire stack. Thus, the transport phenomena in the fuel cell stack, from the viewpoint of their scales of occurrence, can be classified into two categories:

- *Local to a cell:* conservation of mass, momentum and species. At this scale, the inherent slenderness in the functional layers of the cell and the relatively impermeable nature of all layers except for the flow field can be exploited to reduce the elliptic PDEs to parabolic counterparts and even ordinary differential equations (ODEs) with significant savings in computational cost [41,45–48].
- *Global to the stack:* conservation of energy and charge. At this scale, we retain the elliptic nature of the PDEs since there is no slenderness that can be exploited at leading-order. (*N.B.*: It should be possible to still reduce the equations, but we shall not pursue that here; see the Conclusions section for a short discussion.)

This in turn suggests that a hybrid modeling strategy based on these two groups should be feasible and allow for significant reduction in computational cost without sacrificing the fidelity of model predictions for the stack. We shall justify the strategy a *posteriori* by comparing the model predictions from the hybrid strategy with solutions from the full non-reduced set of equations.

To demonstrate the proposed hybrid methodology, we consider a two-dimensional (2D) PEMFC stack system comprising n number of single cells and $n-1$ number of liquid coolant plates (Fig. 1); and the single-phase steady-state model [41,45] that accounts for conservation of mass, momentum, species (O_2, H_2O and N_2 in the cathode; H_2, H_2O and N_2 in the anode), energy, and charge (see Appendix A). The cells are equipped with porous-type flow fields for reactant gases as well as for coolant plates and are operating in coflow mode. We use porous flow fields in order to exploit the fact that they can conveniently be reduced from three dimensions (3D) to two dimensions (2D) and note that the other types of common flow fields – parallel and serpentine flow fields – can also be represented by porous counterparts through spatial smoothing [25,48,49]. As discussed earlier, the governing equations for conservation of mass, momentum, and species can be reduced to a set of parabolic PDEs in the flow fields, and ODEs in the other functional layers (see Appendix B). We refer to [45] for detailed discussion on the reduction methodology and validation with experiments; and [41,45] for other model details – boundary conditions, constitutive equations and base case parameters. (*N.B.*: The strategy is generic and can be extended to account for multiphase flow or 3D geometries that cannot be reduced to 2D.)

3. Hybrid coupling methodology

To couple the solutions for the dependent variables at the local and global level, we iterate between the two as illustrated in the flowchart in Fig. 2. In essence, the following steps are carried out:

1 The local dependent variables in the form of reduced equations are solved; here, we solve reduced equations for the global variables as well to find good initial guesses for the elliptic solver (not necessary, but does speed up overall calculations).

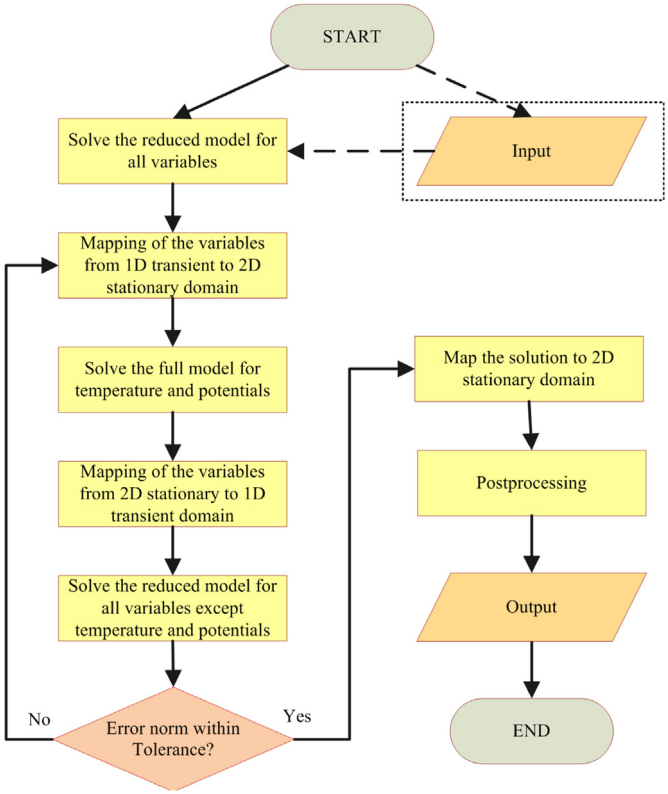

Fig. 2. Flowchart for hybrid simulation strategy for fuel cell stacks.

2 The distributions of the local dependent variables are mapped to a geometry and computational mesh for the solver of the global dependent variables: energy and charge transport.
3 The global dependent variables are solved.
4 The global dependent variables are mapped to the geometry and computational mesh for the local dependent variables.
5 Step 1 is repeated without solving for temperature and charge, which are evaluated from the mapped solution obtained by step 4.
6 Step 2–5 are repeated until the relative error between successive iterations for each variable is less than the specified tolerance.
7 Finally, the solutions for all dependent variables are mapped to geometry for postprocessing.

4. Numerics

The commercial finite-element solver, Comsol 3.5a [50], which allows for the solution of generic differential equations, was employed to solve the 2D full and hybrid models. The elliptic equations in the full model as well as in the hybrid model were solved with an elliptic solver that resolves both the space dimensions altogether, whereas the reduced set of equations (parabolic PDEs and ODEs) was solved by resolving the y-direction as the computational domain and then marching along the x-direction with a space marching algorithm using a transient solver. In other words, the local dependent variables were solved on a 1D transient domain and the global variables on a 2D stationary domain.

A total of 62 mesh elements were used in the y-direction for each cell in the stack (both in full and reduced model) and 60 elements in the x-direction for the full set, whereas the reduced model is simulated for 120 time steps in the x-direction treating x as a timelike variable. The direct solver, Pardiso was chosen as the linear solver for the full non-reduced equations in both the full and hybrid model. For the reduced set of equations, we chose Umfpack as the linear solver and backward differentiation formula with adaptive time stepping as the space marching scheme. Quadratic Lagrange elements were employed with a relative convergence tolerance of 10^{-4} for all variables. Further, solutions from all the models were tested for mesh independence.

We employed automated model generation [41] to build the numerical stack models both for full and reduced set of equations by exploiting the bidirectional interface between Comsol and Matlab [51]. In brief, the automated procedure in the form of a Matlab script manipulates Comsol-associated structures, called the FEM structures that contain the numerical formulation of the entire model, and automates the steps that are necessary to obtain numerical solutions of the mathematical model: viz., drawing the geometry, meshing, implementing the mathematical equations, solving, and post-processing. This approach thus allows for a large reduction in time, since the time spent on manually setting up and solving large stacks is shortened considerably.

The hybrid stack model couples the two FEM structures according to the methodology described in the last *section*. For bijective mapping of the dependent variables from one domain to another, the same number of elements (mesh points) are assigned in the y-direction, and the output times for the transient solver are chosen accordingly. Further, the solutions on the Lagrange nodes are stored in different order for the two domains: as a vector for 2D stationary and as a matrix for 1D transient. Hence, we permute the solution from the source domain to the order of the destination domain while mapping the solutions. The convergence criterion for the hybrid strategy was computed as the weighted Euclidean norm [50],

$$\varepsilon = \sqrt{\frac{1}{N}\sum_{i=0}^{N}(|E_i|/W_i)^2}, \quad (1)$$

where N is the number of degrees of freedom, E_i is the estimated absolute error between iterations, W_i is defined as $\max(U_i,S_i)$, where U_i is the current solution, and S_i was set to 0.1 of the mean of the solution.

All computations were carried out on a workstation with a hexacore processor of 12 threads (3.2 GHz) and a total of 64 GB random access memory (RAM). The peak memory usage was estimated from the task manager taking the difference of idle computer memory and the peak memory during the simulation runs. The real execution times (wall-clock time) were determined from MATLAB's *tic-toc* commands with all unnecessary processes stopped to ensure reasonably accurate estimates.

Finally, we note that the hybrid strategy does not rely on the finite-element as such; the strategy could be implemented with other numerical techniques as well, such as the finite-difference and finite-volume method. Furthermore, one could implement the reduced and full set of equations in a high-level programming language such as Fortran or C; and implement numerical algorithms based on, e.g., a Keller box or a modified box method.

5. Verification

So far, we have employed an understanding of transport phenomena scales – local to a cell or global to the stack – to propose a hybrid-modeling and simulation strategy for fuel cell stacks. Now, in order to verify that the hybrid model does indeed capture the behavior of the full model with redistribution of current and heat flux for the stack, we proceed by considering a 10-cell PEMFC stack operating under non-identical operating conditions. In this regard, we introduce a leading-order perturbation in the inlet velocities for the cathodes, given by

$$U_{c,j}^{in} = U_c^{in} + j\Delta U, \quad (2)$$

where j denotes the number of the cell in the stack, $U_{c,j}^{in}$ is the inlet velocity at the cathode of cell j, $U_c^{in} = 1\ \mathrm{ms}^{-1}$, and ΔU is the increment in inlet velocity from cell to cell. For demonstration purposes, ΔU is chosen such that the inlet velocity increases by a factor of 2 between the first and the last cell, which is larger than the typical variation in inlet velocities between 5 and 25% that have been studied for stacks comprising 25 to 100 cells [21,22,52].

We start by comparing the global behavior in the form of polarization curves predicted by the models based on the full and hybrid sets of equations, as shown in Fig. 3. Overall, the agreement is good with a maximum relative error less than 1%. Similarly, and most importantly, the redistribution of the current density and the temperature distribution between cells in the stack due to the perturbed inlet velocities at the cathodes is captured with a maximum relative error less than 1%; see Figs. 4 and 5 for the first, fifth, and tenth cell in the stack at an operating voltage of 3 V. The

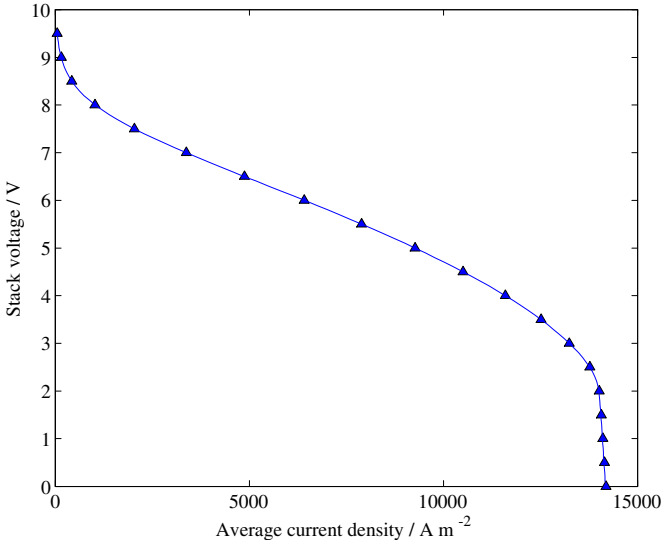

Fig. 3. Polarization curve for a 10-cell stack with perturbed cathode inlet velocities; symbols for the full model and lines for the hybrid counterpart.

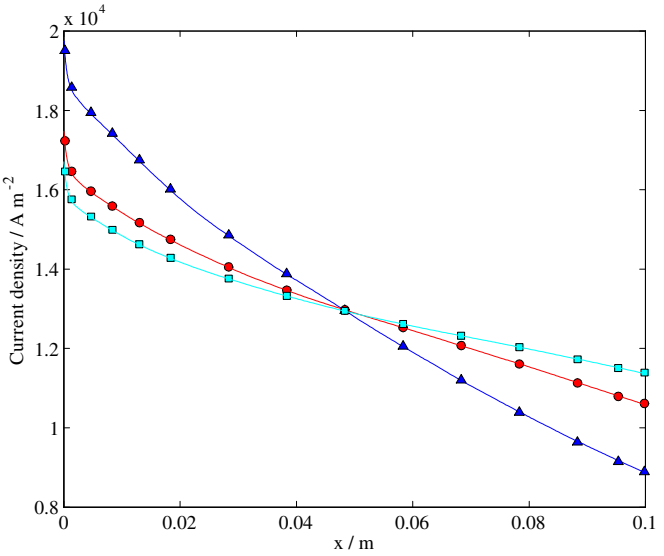

Fig. 4. Local current density distributions for a 10-cell stack ($E_{stack} = 3$ V) along the x-axis at the interface between the cathode catalyst layer and the membrane for the full set of equations in cell (▲) 1, (•) 5, (■) 10; and corresponding predictions of the hybrid set in lines.

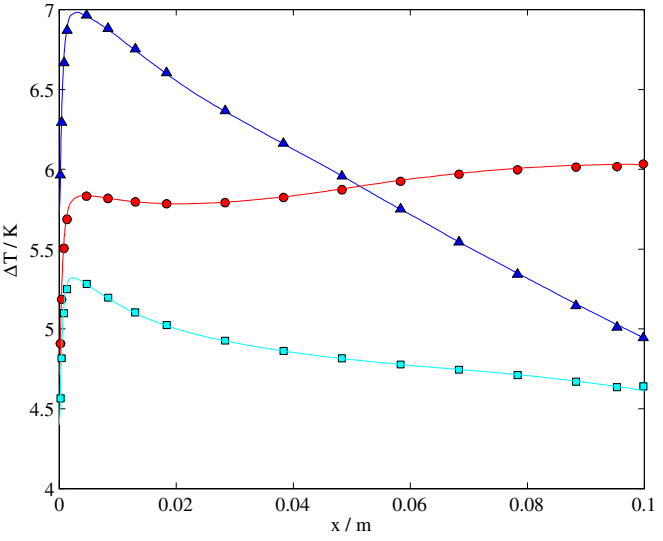

Fig. 5. Local temperature distributions for a 10-cell stack ($E_{stack} = 3$ V) along the x-axis at the interface between the cathode catalyst layer and the membrane for the full set of equations in cell (▲) 1, (•) 5, (■) 10; and corresponding predictions of the hybrid set in lines.

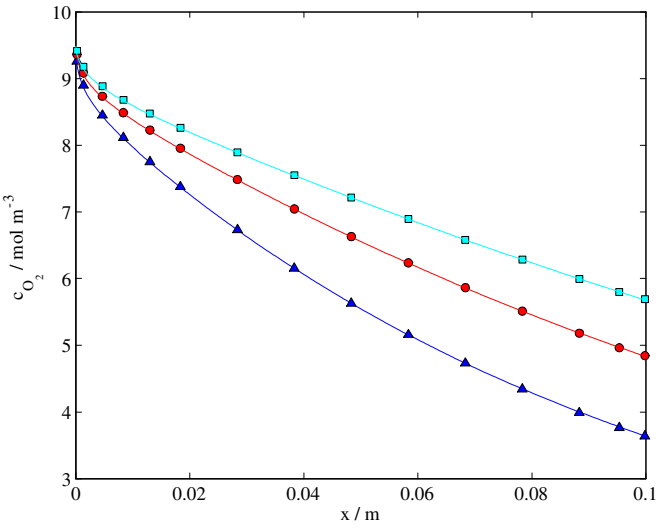

Fig. 6. Local oxygen concentration distributions for a 10-cell stack ($E_{stack} = 3$ V) along the x-axis at the interface between the cathode catalyst layer and the membrane for the full set of equations in cell (▲) 1, (•) 5, (■) 10; and corresponding predictions of the hybrid set in lines.

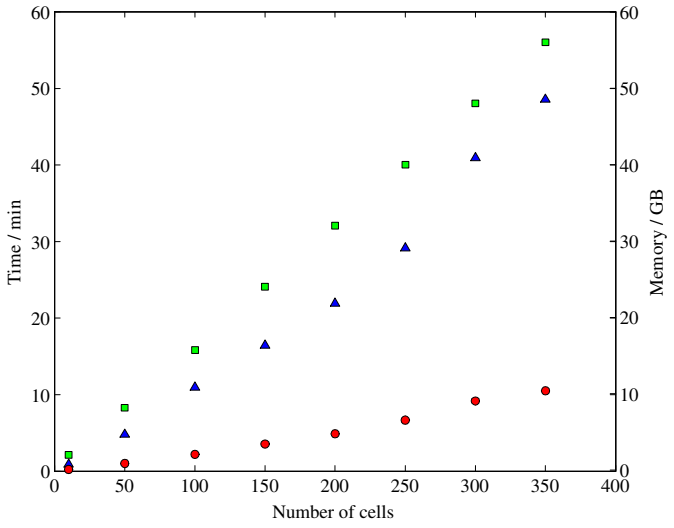

Fig. 7. Scale-up tests for the hybrid model: (■) memory usage, (•) time for setting up the numerical stack models, and (▲) convergence time (at a typical operating voltage of roughly 0.6 V for each cell).

stack voltage is chosen to be in the concentration polarization region, which is the most nonlinear operating regime that corresponds to high current densities with larger spatial variations in the dependent variables. The hybrid strategy has thus removed the limitation of the earlier derived stack model [41], which could not capture the redistribution across the cells.

Finally, let us verify the local dependent variables that were solved with reduced governing equations. We do so for the oxygen concentration in Fig. 6 and again find good agreement with the predicted distribution from the full set of non-reduced equations; the other dependent variables show the same agreement, but are not shown here for the sake of brevity.

6. Computational cost and efficiency

Now that the fidelity of the hybrid model has been verified, let us proceed to address the computational cost and scalability. We expect that the hybrid strategy should lead to significant computational savings as compared to simply solving the full set of equations both in terms of memory and convergence time. This is indeed the case, as can be seen in Table 1, which compares the degrees of freedom (DoF), memory requirement and the time required to reach the converged solution for the full model and hybrid counterpart for three different stacks, comprising 2, 5, and 10 cells, respectively. All stacks are simulated for the same amount of perturbation in cathode inlet velocities across the stack, i.e., the inlet velocity increases by a factor of 2 between the first and the last cell. The DoFs for the hybrid strategy decrease as compared to the full set of equations which leads to substantial savings in the convergence time and memory requirements. Generally speaking, we find that around 80% less memory and execution time is needed for hybrid simulations than for full model simulations for stack sizes up to around 10 cells: e.g., a 10-cell stack at 6 V can be simulated within 1 min and 2 GB of RAM with the hybrid strategy as compared to 6 min and 9 GB of RAM for the full counterpart. As the operating potential decreases, the mathematical equations become more nonlinear rendering the model more difficult to solve, which is evident from the increased computational time for both the models at lower voltages.

Table 1
Computational cost for the full and hybrid sets; the numbers in the brackets indicate the time required to automatically generate the numerical stack model before solving it.

		Full set	Hybrid set
2-Cell stack	DoF	1.5×10^5	6.1×10^4
	Time (s) for 1.6, 1.2, 0.8 V	(*3*) 39,57, 110	(*3*) 9,13,18
	Memory (GB)	2.2	0.67
5-Cell stack	DoF	3.9×10^5	1.6×10^5
	Time (s) for 4, 3, 2 V	(*6*) 130,150, 340	(*7*) 26,27,39
	Memory (GB)	5	1.2
10-Cell stack	DoF	7.8×10^5	3.1×10^5
	Time (s) for 8, 6, 4 V	(*11*) 210,330, 750	(*13*) 35,53, 82
	Memory (GB)	9	2

On our workstation, the computational cost for the full model becomes prohibitive for stacks with 50 or more cells, unless one switches to iterative solvers that are less robust and need fine-tuning. However, the hybrid strategy can simulate the behavior of stacks up to around 350 cells with a robust solver as depicted in Fig. 7. Here, we see that the computational cost in terms of memory usage, time required for setting up the models (done automatically with the automated code generator), and convergence time increase roughly linearly with the number of cells. One could pursue larger stacks by switching to an iterative solver for the global variables governed by elliptic PDEs in order to decrease the memory requirements—doing so would be at the expense of robustness, however.

7. Conclusions

We have proposed and demonstrated a hybrid strategy to tackle the prohibitive computational costs of solving detailed mechanistic models for fuel cell stacks whilst capturing the essential physics—in particular the redistribution of current and heat flux between cells in a perturbed stack.

In essence, the strategy relies on exploiting the scales and nature of the dependent variables: chemical species, momentum and mass are local to cells and their governing equations can be reduced mathematically by invoking the slenderness and impermeable nature of the functional layers found at the cell level; whereas charge and temperature are global to the stack, and thus retain

their elliptic nature. The strategy was verified with good agreement by comparing with solutions obtained from solving the non-reduced full set of equations.

Around 80% computational savings both in terms of memory usage and execution time were achieved with the hybrid strategy for stacks up to around 10 cells. In addition, the strategy allows for the simulation of larger stacks: e.g., it took less than an hour to simulate a perturbed 350-cell stack. The scalability and associated low computational cost should allow for various applied studies on fuel cell stacks e.g., modeling of statistical and/or random variations and perturbations in the operating conditions and material properties arising during manufacture and assembly, establishing quality control guidelines for rejection or acceptance of a cell during assembly, and optimizing operating and design parameters for a stack.

Here, we solve the full set of equations for energy and charge transport coupled with the reduced equations for other transport processes. Another possible approach could be to continue with the asymptotically reduced equations for all the transport phenomena augmented with the next-order solutions of their asymptotic series to resolve the redistribution of the energy and charge between the cells. An alternate strategy could be to secure analytical solutions of the elliptic governing equations for charge and energy and couple these with the reduced formulation for the local dependent variables.

On a final note, the classification of transport phenomena based on their scales and associated model reductions for the local variables is a fundamental concept and could thus be extended to 3D models and other electrochemical systems, such as batteries, flow batteries, and supercapacitors. Furthermore, the strategy is not limited to electrochemical stacks, but could also be applied to other systems that exhibit some degree of slenderness for local variables: e.g., in catalytic monolith reactors comprising multiple slender channels where the mass, momentum, and species transport are limited to single channels but the heat transport occurs throughout the reactor.

Acknowledgments

This research is supported by the National Research Foundation, Singapore under its Competitive Research Program (Award No. NRF-CRP8-2011-04). The authors would also like to acknowledge the support of National University of Singapore.

Appendix A. Full set of governing equations

We consider conservation of mass, momentum, species, energy and charge in the PEMFC, expressed as

$$\nabla\cdot(\rho\mathbf{v}) = S_{\text{mass}}, (\text{ff},\ \text{pb},\ \text{cl},\ \text{el}) \tag{A.1}$$

$$\nabla p = -\frac{\mu}{\kappa}\mathbf{v} + \mathbf{S}_{\text{mom}}, (\text{ff},\ \text{pb},\ \text{cl},\ \text{el}) \tag{A.2}$$

$$\nabla\cdot\mathbf{N}_{\text{i}} = S_{\text{i}}, (\text{ff},\ \text{pb},\ \text{cl},\ \text{el}) \tag{A.3}$$

$$\rho c_{\text{p}}\mathbf{v}\cdot\nabla T = \nabla\cdot\left(k^{\text{eff}}\nabla T\right) + S_{\text{temp}}, (\text{everywhere}) \tag{A.4}$$

$$\nabla\cdot\mathbf{i}_{\text{m}} = S_{\text{pot}}, (\text{cl},\ \text{el}) \tag{A.5}$$

$$\nabla\cdot\mathbf{i}_{\text{s}} = -S_{\text{pot}}, (\text{sp},\ \text{ff},\ \text{pb},\ \text{cl}) \tag{A.6}$$

where the molar fluxes of species, $\mathbf{N}_{\text{i}}$ and current densities, $\mathbf{i}$ are defined as

$$\mathbf{N}_{\text{O}_2} = c_{\text{O}_2}\mathbf{v} - D^{\text{eff}}_{\text{O}_2}\nabla c_{\text{O}_2},\ (\text{ff},\ \text{pb},\ \text{cl}\ \text{ in the cathode}) \tag{A.7}$$

$$\mathbf{N}_{\text{H}_2} = c_{\text{H}_2}\mathbf{v} - D^{\text{eff}}_{\text{H}_2}\nabla c_{\text{H}_2},\ (\text{ff},\ \text{pb},\ \text{cl in the anode}) \tag{A.8}$$

$$\mathbf{N}_{\text{H}_2\text{O}} = \begin{cases} \frac{n_{\text{d}}\mathbf{i}_{\text{m}}}{F} - \frac{\rho_{\text{m}}}{M_{\text{m}}}D_{\text{H}_2\text{O,m}}\nabla\lambda & (el) \\ c_{\text{H}_2\text{O}}\mathbf{v} - D^{\text{eff}}_{\text{H}_2\text{O}}\nabla c_{\text{H}_2\text{O}} & (\text{elsewhere}) \end{cases}, \tag{A.9}$$

$$\mathbf{i}_{\text{m}} = -\sigma_{\text{m}}\nabla\phi_{\text{m}}, \tag{A.10}$$

$$\mathbf{i}_{\text{s}} = -\sigma_{\text{s}}\nabla\phi_{\text{s}}. \tag{A.11}$$

For the coolant flow fields, we only need to consider conservation of energy and charge, which can be written as

$$\rho^{(\text{l})}c_{\text{p}}^{(\text{l})}U^{\text{cool}}\mathbf{e}_x\cdot\nabla T = \nabla\cdot\left(k^{\text{eff}}\nabla T\right) + S_{\text{temp}},\ (\text{cff}) \tag{A.12}$$

$$\nabla\cdot(-\sigma_{\text{s}}\nabla\phi_{\text{s}}) = 0\ (\text{cff}) \tag{A.13}$$

In the above equations, ρ is the density, $\mathbf{v}$ is the velocity, p is the pressure, μ is the dynamic viscosity, κ is the hydraulic permeability of the porous medium, c_{p} is the specific heat capacity, T is the temperature, k^{eff} is the effective thermal conductivity, $\mathbf{i}_{\text{m}}$ is the ionic current density, and $\mathbf{i}_{\text{s}}$ is the electronic current density. In the molar flux of species (Eqs. A.7 and A.8), c_{i} and $D^{\text{eff}}_{\text{i}}$ denote the molar concentration and effective diffusivity of species i. The flux of water in the membrane (Eq. (A.9)) due to electro-osmotic drag and diffusion is expressed using a phenomenological model [53] in terms of the membrane water content, λ where n_{d} is electroosmotic drag coefficient, $\mathbf{i}_{\text{m}}$ is the current density carried by protons, F is Faraday's constant, $D_{\text{H}_2\text{O,m}}$ is the diffusivity of water in the membrane, ρ_{m} and M_{m} are the density and equivalent weight of the dry membrane, respectively. In the flux of current density (Eqs. A.10 and A.11), φ_{m} represents the potential of the ionic phase and φ_{s} the solid phase; σ_{m} and σ_{s} are the electrical conductivities of proton and electron transport, respectively. In Eq. (A.12), $\rho^{(\text{l})}$ and $c_{\text{p}}^{(\text{l})}$ are the density and the specific heat capacity of the liquid coolant (H_2O in this case), U^{cool} is the average velocity of the flow through the porous coolant plates (N.B. for passive flow in a channel comprising a porous medium with slip-conditions, a constant velocity profile is obtained, which is given by U^{cool} in Eq. (A.12)), and $\mathbf{e}_x$ is the streamwise coordinate vector.

Appendix B. Reduced equations for conservation of mass, momentum, and species

We solve for the conservation of mass and momentum, given by

$$\frac{\partial p}{\partial x} = -\frac{\mu}{\kappa\rho}\frac{\partial\psi}{\partial y} - \frac{c_{\text{F}}}{\sqrt{\kappa}\rho}\left(\frac{\partial\psi}{\partial y}\right)^2,\ (\text{ff}) \tag{B.1}$$

$$\frac{\partial p}{\partial y} = 0,\ (\text{ff}) \tag{B.2}$$

$$\frac{\partial}{\partial y}(\rho v) = S_{\text{mass}},\ (\text{pb},\ \text{cl},\ \text{el}) \tag{B.3}$$

$$\frac{\partial p}{\partial y} = -\frac{\mu}{\kappa} v, (\text{pb, cl, el}) \quad \text{(B.4)}$$

The streamfunctions, ψ, are defined through

$$u = \frac{1}{\rho}\frac{\partial \psi}{\partial y}, \quad v = -\frac{1}{\rho}\frac{\partial \psi}{\partial x}, \quad \text{(B.5)}$$

such that they satisfy conservation of mass in the flow fields; here, u and v are the velocities in the x- and y-direction, respectively. Note that we solve for ψ and p in the flow fields, in lieu of u, v, and p, whereas we solve for v and p in the gas diffusion layer, catalyst layers and membranes. The second term in right hand side of Eq. B.1 originates from the momentum source, S_{mom}; refer to [41] for details.

The reduced equations for the conservation of species can be expressed as

$$\frac{\partial}{\partial x}(c_i u) + \frac{\partial}{\partial y}(c_i v) = \frac{\partial}{\partial y}\left(D_i^{eff}\frac{\partial c_i}{\partial y}\right), \quad (\text{ff}) \quad \text{(B.6)}$$

$$\frac{\partial}{\partial y}(c_i v) = \frac{\partial}{\partial y}\left(D_i^{eff}\frac{\partial c_i}{\partial y}\right) + S_i, \quad (\text{pb, cl}) \quad \text{(B.7)}$$

$$\frac{\partial}{\partial y}\left(\frac{n_d i_m}{F}\right) = \frac{\partial}{\partial y}\left(\frac{\rho_m}{M_m} D_{H_2O,m}\frac{\partial \lambda}{\partial y}\right), \quad (\text{m}) \quad \text{(B.8)}$$

List of symbols

c_F	form-drag constant
c_i	molar concentration of species i, mol m^{-3}
c_p	specific heat capacity, J kg^{-1} K^{-1}
D_i	diffusivity of species i, m^2 s^{-1}.
$D_{H_2O,m}$	diffusivity of water in the membrane, m^2 s^{-1}
$\mathbf{e}_x$, $\mathbf{e}_y$, $\mathbf{e}_z$	coordinate vectors
E_{stack}	stack voltage, V
F	Faraday's constant, A s mol^{-1}
i,$\mathbf{i}$	current density, A m^{-2}
j	building block
k	thermal conductivity, W m^{-1} K^{-1}
M_m	equivalent weight of the dry membrane, kg mol^{-1}
n	the number of cells
n_d	electroosmotic drag coefficient
$\mathbf{N}_i$	molar flux of species i, mol m^{-2} s^{-1}
p	pressure, Pa
S	source term
T	temperature, K
u,v,$\mathbf{v}$,U	velocities, m s^{-1}
x,y,z	coordinate, m

Greek

κ	permeability, m^2
λ	water content
μ	dynamic viscosity, kg m^{-1} s^{-1}
ρ	density, kg m^{-3}
σ_m	protonic conductivity, S m^{-1}
σ_s	electric conductivity, S m^{-1}
φ	potential, V
ψ	stream function

Superscripts

cool	cooling
eff	effective
(l)	liquid

Subscripts

H_2	hydrogen
H_2O	water
i	species i
m	membrane
mass	mass
mom	momentum
N_2	nitrogen
O_2	oxygen
pot	potential
s	solid phase
temp	temperature

References

[1] C.-Y. Wang, Chem. Rev. 104 (2004) 4727–4765.
[2] K. Yao, K. Karan, K. McAuley, P. Oosthuizen, B. Peppley, T. Xie, Fuel Cells 4 (2004) 3–29.
[3] D. Cheddie, N. Munroe, J. Power Sources 147 (2005) 72–84.
[4] H. Liu, T. Zhou, P. Cheng, J. Heat Transfer 127 (2005) 1363–1379.
[5] S. Kakac, A. Pramuanjaroenkij, X.Y. Zhou, Int. J. Hydrogen Energy 32 (2007) 761–786.
[6] V. Oliveira, D. Falcoa, C. Rangel, A. Pinto, Int. J. Hydrogen Energy 32 (2007) 415–424.
[7] C. Siegel, Energy 33 (2008) 1331–1352.
[8] K. Wang, D. Hissel, M. Pera, N. Steiner, D. Marra, M. Sorrentino, C. Pianese, M. Monteverde, P. Cardone, J. Saarinen, Int. J. Hydrogen Energy 36 (2011) 7212–7228.
[9] Z. Liu, Z. Mao, C. Wang, W. Zhuge, Y. Zhang, J. Power Sources 160 (2) (2006) 1111–1121.
[10] Y. Shan, S.-Y. Choe, S.-H. Choi, J. Power Sources 165 (1) (2007) 196–209.
[11] S. Shimpalee, M. Ohashi, J.V. Zee, C. Ziegler, C. Stoeckmann, C. Sadeler, C. Hebling, Electrochim. Acta 54 (10) (2009) 2899–2911.
[12] I.B. Celik, S.R. Pakalapati, From a Single Cell to a Stack Modeling, Springer Science+Business Media B.V, 2008, pp. 123–182 (Chapter 5).
[13] C.-H. Cheng, H.-H. Lin, J. Power Sources 194 (2009) 349–359.
[14] A.D. Le, B. Zhou, J. Power Sources 195 (2010) 5278–5291.
[15] A.P. Sasmito, E. Birgersson, A.S. Mujumdar, Heat Transfer Eng. 32 (2011) 151–167.
[16] M. Kvesic, U. Reimer, D. Froning, L. Luke, W. Lehnert, D. Stolten, Int. J. Hydrogen Energy 37 (2012) 2430–2439.
[17] M. Kvesic, U. Reimer, D. Froning, L. Lke, W. Lehnert, D. Stolten, Int. J. Hydrogen Energy 37 (2012) 12438–12450.
[18] S. Zhai, S. Zhou, F. Chen, P. Sun, K. Sundmacher, J. Fuel Cell Sci. Technol. 9 (2012) 011014-1.
[19] P. Argyropoulos, K. Scott, W. Taama, J. Power Sources 79 (1999) 169–183.
[20] P. Argyropoulos, K. Scott, W. Taama, J. Power Sources 79 (1999) 184–195.
[21] P.A. Chang, J. St-Pierre, J. Stumper, B. Wetton, J. Power Sources 162 (2006) 340–355.
[22] C.-H. Chen, S.-P. Jung, S.-C. Yen, J. Power Sources 173 (2007) 249–263.
[23] A.A. Kulikovsky, J. Electrochem. Soc. 153 (9) (2006) A1672–A1677.
[24] A. Kulikovsky, Electrochim. Acta 53 (22) (2008) 6391–6396.
[25] J. McIntyre, A.A. Kulikovsky, M. Müller, D. Stolten, Fuel Cells 12 (6) (2012) 1032–1041.
[26] J. McIntyre, A.A. Kulikovsky, M. Müller, D. Stolten, Int. J. Hydrogen Energy 38 (2013) 3373–3379.
[27] S. Beale, Y. Lin, S. Zhubrin, W. Dong, J. Power Sources 118 (1–2) (2003) 79–85.
[28] A. Burt, I. Celik, R. Gemmen, A. Smirnov, J. Power Sources 126 (1–2) (2004) 76–87.
[29] A. Smirnov, A. Burt, I. Celik, J. Power Sources 158 (1) (2006) 295–302.
[30] D.L. Damm, A.G. Fedorov, J. Power Sources 159 (2) (2006) 956–967.
[31] S. Philipps, C. Ziegler, J. Power Sources 180 (2008) 309–321.
[32] Y.-W. Kang, J. Li, G.-Y. Cao, H.-Y. Tu, J. Li, J. Yang, J. Power Sources 188 (1) (2009) 170–176.
[33] K. Lai, B.J. Koeppel, K.S. Choi, K.P. Recknagle, X. Sun, L.A. Chick, V. Korolev, M. Khaleel, J. Power Sources 196 (2011) 3204–3222.
[34] R. Cozzolino, S. Cicconardi, E. Galloni, M. Minutillo, A. Perna, Int. J. Hydrogen Energy 36 (13) (2011) 8030–8037.
[35] M. Khandelwal, S. Lee, M. Mench, J. Power Sources 172 (2007) 816–830.
[36] M. Khandelwal, M. Mench, J. Power Sources 195 (2010) 6549–6558.
[37] J. Ramousse, K.P. Adzakpa, Y. Dub, K. Agbossou, M. Fournier, A. Poulin, M. Dostie, J. Fuel Cell Sci. Technol. 7 (2010) 041006-1.
[38] A.A. Kulikovsky, SIAM J. Appl. Math. 70 (2009) 531–542.
[39] A.A. Kulikovsky, J. Electrochem. Soc. 157 (4) (2010) B572–B579.

[40] N. Akhtar, S.P. Decent, D. Loghin, K. Kendall, Int. J. Hydrogen Energy 34 (2009) 8645–8663.
[41] H. Ly, E. Birgersson, M. Vynnycky, J. Electrochem. Soc. 157 (2010) B982–B992.
[42] G.-S. Kim, J. St-Pierre, K. Promislow, B. Wetton, J. Power Sources 152 (2005) 210–217.
[43] P. Berg, A. Caglar, K. Promislow, J. St-Pierre, B. Wetton, IMA J. Appl. Math. 71 (2) (2006) 241–261.
[44] A.A. Kulikovsky, J. Electrochem. Soc. 154 (8) (2007) B817–B822.
[45] H. Ly, E. Birgersson, M. Vynnycky, A.P. Sasmito, J. Electrochem. Soc. 156 (2009) B1156–B1168.
[46] S.L. Ee, E. Birgersson, J. Electrochem. Soc. 156 (11) (2009) B1329–B1338.
[47] S.L. Ee, E. Birgersson, J. Electrochem. Soc. 158 (10) (2011) B1224–B1234.
[48] Z. He, H. Li, E. Birgersson, Comput. Chem. Eng. 52 (2013) 155–167.
[49] H. Ly, E. Birgersson, M. Vynnycky, Int. J. Hydrogen Energy 37 (2012) 7779–7795.
[50] COMSOL Multiphysics 3.5a, http://www.comsol.com.
[51] MATLAB R2011b, http://www.mathworks.com.
[52] R. Mustata, L. Valio, F. Barreras, M.I. Gil, A. Lozano, J. Power Sources 192 (2009) 185–189.
[53] T.E. Springer, T.A. Zawodzinski, S. Gottesfeld, J. Electrochem. Soc. 138 (1991) 2334–2342.